Pelagic and coastal sources of *P*-wave microseisms: Generation under tropical cyclones

Jian Zhang,[1] Peter Gerstoft,[1] and Peter D. Bromirski[1]

Received 9 June 2010; revised 29 June 2010; accepted 7 July 2010; published 6 August 2010.

[1] Nonlinear wave-wave interactions generate double-frequency (DF) microseisms, which include both surface waves (mainly Rayleigh-type) and compressional (*P*) waves. Although it is unclear whether DF surface waves generated in deep oceans are observed on land, we show that beamforming of land-based seismic array data allows detection of DF *P* waves generated by ocean waves from Super Typhoon Ioke in both pelagic and coastal regions. Two distinct spectral bands associated with different *P*-wave source locations are observed. The short-period DF band (0.16–0.35 Hz) is dominated by *P* waves generated in the deep ocean by local wind seas under the storm. In contrast, *P* waves in the long-period DF band (0.1–0.15 Hz) are weaker and generated closer to the coast of Japan from swell interactions. The accurate identification of DF *P*-wave microseism source areas is useful to monitor ocean wave-wave interactions due to tropical cyclones and to image Earth structure using ambient seismic noise. **Citation:** Zhang, J., P. Gerstoft, and P. D. Bromirski (2010), Pelagic and coastal sources of *P*-wave microseisms: Generation under tropical cyclones, *Geophys. Res. Lett.*, *37*, L15301, doi:10.1029/2010GL044288.

1. Introduction

[2] Microseisms are the small and continuous ground vibrations detected by seismometers worldwide. Broadband seismic spectra commonly exhibit prominent peaks due to ocean waves, namely primary (or single-frequency, SF, from about 0.05 to 0.1 Hz) and secondary (or double-frequency, DF, from about 0.1 to 0.5 Hz) microseisms. SF microseisms are generated only in shallow water through shoaling and breaking of ocean waves. Nonlinear wave-wave interactions generate a standing wave pressure excitation pulse at twice the ocean-wave frequency [*Longuet-Higgins*, 1950] that excites DF microseisms at the seafloor. DF microseisms can be classed as long-period DF (LPDF, or low-frequency DF, generated by swells) and short-period DF (SPDF, or high-frequency DF, generated by local wind seas) microseisms [*Bromirski et al.*, 2005].

[3] Locating DF microseism source areas is important to evaluate seafloor sites for earthquake detection, and also to image Earth structure by using ambient noise [e.g., *Shapiro et al.*, 2005; *Sabra et al.*, 2005; *Zhang et al.*, 2010]. Most DF microseism observations indicate near-coastal shallow-water source areas [e.g., *Haubrich and McCamy*, 1969; *Bromirski and Duennebier*, 2002; *Bromirski et al.*, 2005; *Tanimoto et al.*, 2006; *Tanimoto*, 2007; *Gerstoft and Tanimoto*, 2007]. However, a few array analyses [e.g., *Cessaro*, 1994; *Chevrot et al.*, 2007] suggest occasional deep-ocean origins. But these studies used only polarization and triangulation methods, with an uncertainty from assuming a common source region for different array sites. *Kedar et al*. [2008] also identified a deep-ocean source area by modeling DF microseism surface waves, but without considering near-coastal generation.

[4] Traditional microseism source localization efforts often consider only surface waves. Microseisms are thought to propagate primarily as Rayleigh waves [e.g., *Sutton and Barstow*, 1990], although careful analysis of microseism mode structure is rare in the literature. In fact, *P* waves generated under storms in deep oceans have been identified as early as the late 1960s [*Burg and Burrell*, 1967; *Toksöz and Lacoss*, 1968; *Haubrich and McCamy*, 1969], but these phases received little attention until Hurricane Katrina "hit" California [*Gerstoft et al.*, 2006]. Microseismic *P* waves are observed across the dominant portion of the DF spectrum, but are often strongest in the SPDF band (0.16–0.35 Hz). Modern array techniques have now allowed observations of significant *P*-wave microseisms that can be associated with sea states and even specific storms [*Gerstoft et al.*, 2008; *Koper and de Foy*, 2008; *Koper et al.*, 2009; *Landes et al.*, 2010].

[5] The goal of this study is to determine if deep-ocean source areas of microseismic *P* waves can be definitively identified using frequency-domain beamforming of land-based seismic array data recorded in California and Japan during a specific western Pacific storm – Super Typhoon Ioke (Figure 1a). The beamformer outputs allow locating the *P*-wave source areas, which are comparable to the storm positions. Such observations indicate that body-wave microseisms generated by energetic nonlinear wave-wave interactions occurring in the deep ocean can be observed on land. In addition, we are able to distinguish distinct SPDF and LPDF *P*-wave microseism source areas through spectral analysis of the beamformer outputs.

2. Data and Processing

[6] Super Typhoon Ioke is the strongest tropical cyclone on record over the western Pacific. Ioke traversed the deep Pacific Ocean for 19 days (August 20 to September 7 in 2006 (see Figure 1a)), making it an ideal candidate for establishing the spatiotemporal correlation between microseismic *P*-wave observations and deep-ocean storms. Continuous vertical-component seismic data recorded at the Southern California Seismic Network (SCSN), as well as the Japanese high-sensitivity seismograph network (Hi-net), were analyzed. To mitigate contamination from occasional large-amplitude transients (e.g., earthquakes), these high amplitude signals

[1]Scripps Institution of Oceanography, University of California, San Diego, La Jolla, California, USA.

0094-8276/10/2010GL044288

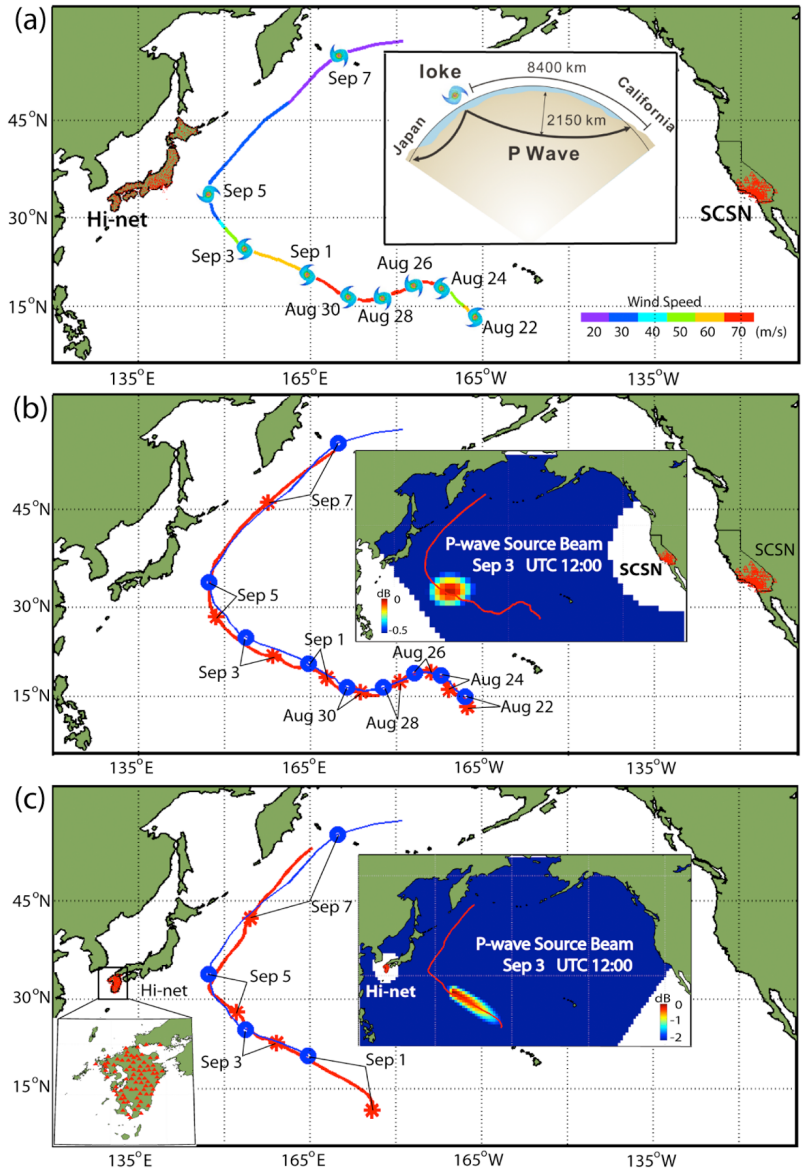

Figure 1. Pelagic *P*-wave microseism sources tailing Super Typhoon Ioke. (a) Locations of the two arrays (SCSN and Hi-net, red), and the best-track of Super Typhoon Ioke (August 22–September 7, from National Hurricane Center http://www.nhc.noaa.gov/), with wind speed indicated (color scale) and a schematic of *P*-wave ray paths from Ioke to California and Japan (insert). (b) Tracks of Ioke (blue) and Ioke-generated SPDF *P*-wave sources (red) using the SCSN stations. Locations of *P*-wave sources (*) and storm centers (o) are marked every second day. The insert shows *P*-wave beamformer output on 3 September. (c) Similar to Figure 1b, but for the beamformer outputs (September 1–7) from using 79 of the southernmost Hi-net stations.

were truncated to the level of the largest microseism amplitude. We also use broadband seismic data from selected stations of the F-net network in Japan for comparative spectral analysis.

[7] Beamforming was done by first constructing the cross-spectral density matrix $\mathbf{C}(\omega,t) = \langle \mathbf{v}(\omega,t)\ \mathbf{v}^{\mathrm{T}}(\omega,t) \rangle$, where $\mathbf{v}(\omega,t)$ is a complex-valued vector of the seismograms from all stations, and $\langle\rangle$ indicates averaging over successive 3-hour windows. The response of the seismic array to each point source over the Earth's global surface is given by $\mathbf{p}(\omega,lat,lon) = \exp(i\omega\, \mathbf{t}_{lat,lon})$, where $\mathbf{t}_{lat,lon}$ describes the travel-time estimates from a grid point to each array stations, using a global *P*-wave travel-time model [e.g., *Kennett et al.*, 1995]. The beamformer output is then given by $b(\omega,t,lat,lon) = \mathbf{p}^{\mathrm{T}}\ (\omega,lat,lon)\ \mathbf{C}(\omega,t)\ \mathbf{p}(\omega,lat,lon)$.

3. Synoptic Observations and Implications

[8] Strong coherent *P* waves generated under Super Typhoon Ioke are revealed and traced back to their origin locations via array beamforming of the microseisms recorded at the SCSN and the Hi-net respectively. First we focus on the SPDF band (about 0.16–0.35 Hz), as the power of *P*-wave beams peaks around 0.2 Hz. Tests show that *P*-wave energy is below the array noise floor at frequencies greater than 0.35 Hz. The trace of *P*-wave source locations,

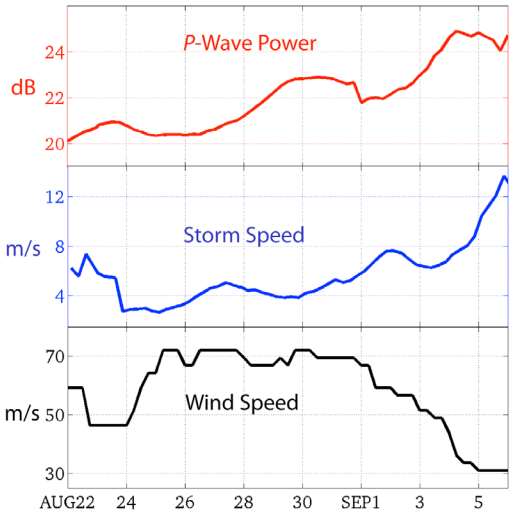

Figure 2. *P*-wave power (estimated using the peak amplitudes of beamformer outputs and corrected for distance-dependent geometric spreading) compared with storm propagation speed and wind speed.

derived from using data at the SCSN, follows the path of Ioke (Figure 1b; typical beamformer output is shown in the insert, see Figure S1 of the auxiliary material for images of every second day).[1] The source locations can also be identified using data from 79 southern stations of the Hi-net (Figure 1c), although the precision is relatively poor, in part due to the array geometry and the relatively short distance of Ioke from the array. Comparison of the *P*-wave source paths with the track of Ioke clearly indicates that these *P* waves originated in the deep ocean near Ioke. This provides direct evidence that nonlinear wave-wave interactions in deep oceans generate *P*-wave microseisms that can be observed by land stations.

[9] Surface-wave microseisms might be generated in deep water near Ioke. A strong localized cyclone that has not yet interacted with the coast should provide a likely scenario for deep-water generation of SPDF surface waves. Deep-water SPDF *P* waves from Ioke were observed in this study, and *Bromirski et al.* [2005] observed deep-water SPDF microseisms at the ocean bottom. However, and in contrast, deep-water generated surface-wave microseisms from Ioke were not identified with the land array data (Figure S2), consistent with studies indicating that non-coastal DF surface-wave microseisms are not observed at land stations [*Bromirski*, 2001; *Bromirski and Duennebier*, 2002; *Gerstoft and Tanimoto*, 2007].

[10] Although the source locations of SPDF *P* waves correlate well with the track of Ioke, they do not necessarily coincide with the locations of the storm center. Disregarding possible beamforming bias due to Earth structure heterogeneity, the locations of the *P*-wave peak beam (thus the field of wave-wave interactions) tend to trail Ioke, i.e., in the storm's wake (Figures 1b and 1c), as also observed by *Haubrich and McCamy* [1969]. Opposing waves may develop behind a storm when it overrides its waves. For example, the western quadrant of Ioke forces wind waves southward. If the storm is moving northward faster than the ocean gravity waves propagate, southward traveling wind waves could interact with previously generated northward propagating wind waves at locations behind the storm. However, during August 22 – September 4, *P* waves at 0.2 Hz were generated near Ioke even when the storm propagation speed was less than the group speed of the deep-water ocean waves at 0.1 Hz, i.e., 8 m/s [$c_{group} = g/(4\pi f)$]. This suggests that there must be some wave-wave interactions due to the inhomogeneity of local wave fields even when the storm is stationary.

[11] Power of the SPDF *P* waves generated by Ioke provides a proxy of the intensity of wave-wave interaction under the storm. We made a correction of the SPDF *P*-wave beam power by considering the distance-dependent geometric spreading for *P* waves in a spherically symmetric Earth [*Shearer*, 2009]. The corrected *P*-wave power is compared with the Ioke propagation speed (estimated from the best-track locations at each 6-h time step) and the maximum wind speed (Figure 2), giving correlation-coefficients of 0.72 and −0.66 respectively. Stronger *P* waves were generated when Ioke propagated faster, suggesting that a faster-moving storm may simply increase the area of wave-wave interactions. The lack of positive correlation between the *P*-wave power and wind speed is consistent with the most intense wave-wave interactions occurring not directly under the storm, but after the waves have propagated some distance where they interact with previously generated waves. However, multiple factors may contribute to the intensity of wave-wave interaction. The magnitude and frequency of ocean waves generated by storms is a function of the wind speed, duration, and fetch, each of which vary. In addition, the estimate of *P*-wave energy generated by the storm can be biased due to scattering and lateral structure dependence of attenuation along the storm track.

[12] Mid-ocean sites exhibit concentrations of DF microseism energy in the SPDF band associated with local wind seas, and in the swell-generated LPDF band linked to near-coastal wave activity [*Bromirski et al.*, 2005]. This can be clearly seen in the spectral variation sampled at three F-net stations in Japan (Figures 3a–3d) when nearby Ioke transited northwards (September 2–6). Both surface waves and *P* waves likely contribute to the microseism levels observed, although their respective contributions to each band are not known. The different levels of power near 0.2 Hz at the three stations result from their proximity to Ioke and the storm strength at its closest approach to the Japanese coast, with a significant contribution from the storm-associated wave-wave activities at nearby shorelines. Because long-period swell propagates with less dissipation, the differences in the LPDF band between the stations are less. The presence of a strong SPDF *P*-wave component in microseisms is also consistent with *Tanimoto et al.* [2006], who found that Rayleigh waves appear less dominant above about 0.2 Hz, potentially because of a strong *P* wave contribution.

[13] Swell wave-wave interactions can occur distant from storms, i.e., when incident swell interacts with swell from coastal reflections or from another storm system. This suggests that the Ioke-generated swell may generate *P* waves in the LPDF band distant from the storm. Two relatively distinct *P*-wave source regions are identified for the LPDF and SPDF bands. The beams were calculated and stacked over

[1] Auxiliary materials are available in the HTML. doi:10.1029/2010GL044288.

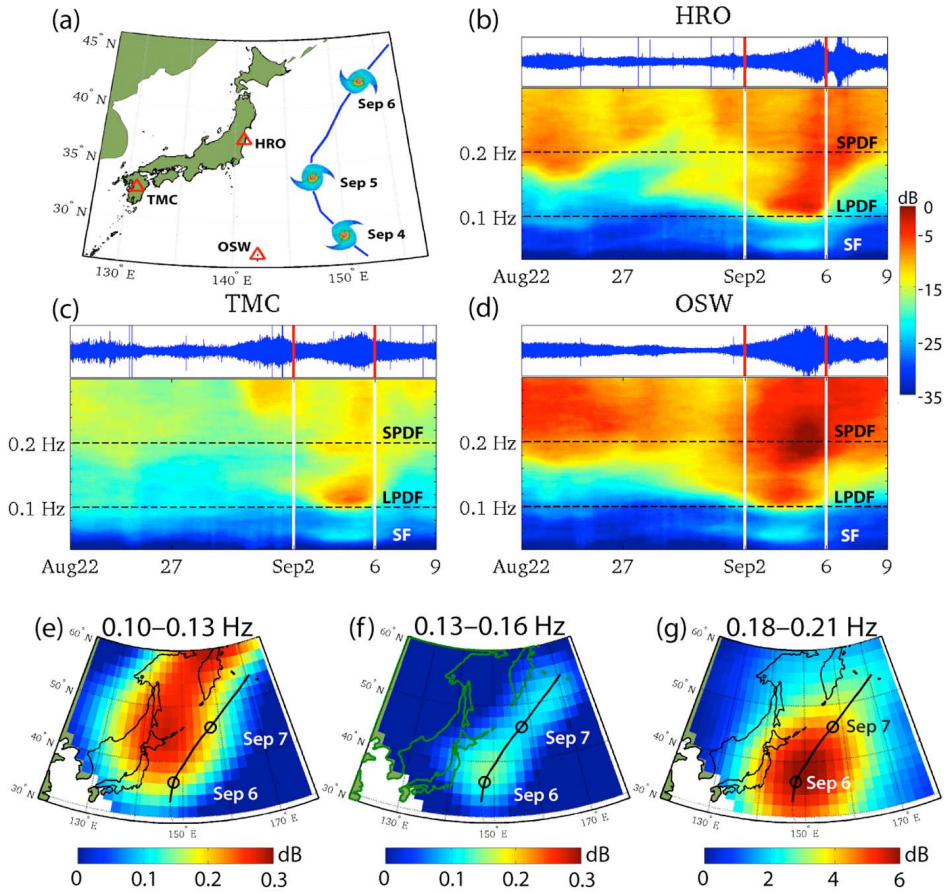

Figure 3. Spectral partitioning of microseismic *P* waves and their sources. (a) Locations of three individual stations (triangles) and track of Ioke (blue trace). (b–d) Vertical-component time series and spectrograms of the data form HRO, TMC, and OSW. Bands associated with single frequency (SF), long-period double frequency (LPDF), and short-period double frequency (SPDF) microseisms are indicated. Beamformer outputs of *P*-wave sources using the SCSN data are shown for three frequency bands: (e) LPDF, 0.10–0.13 Hz, (f) 0.13–16 Hz, and (g) SPDF, 0.18–0.21 Hz. The beam is averaged over UTC 12-h September 5 through September 7. The trace and circles indicate the temporal locations of the SPDF *P*-wave sources. Note that the beam power is significantly higher in the SPDF band.

the 0.10–0.13 Hz, 0.13–0.16 Hz, and 0.18–0.21 Hz when Ioke was weakening. LPDF *P*-wave microseisms tend to be generated closer to the coast (Figure 3e), which is clearly distinct from the deep-ocean SPDF *P*-wave source area near the storm (Figure 3g). Note that the power of the LPDF *P* waves is much less than the SPDF *P* waves. Relatively little *P*-wave energy was generated in the mid-range DF band (Figure 3f), in agreement with the spectral minimum in this band (Figures 3b–3d) [*Bromirski et al.*, 2005].

4. Seasonal Variability of *P*-Wave Microseism Source Areas

[14] Observations over the whole year 2006 show a seasonal variability of *P*-wave microseism source areas. The dominant SPDF *P*-wave source areas occur in deep oceans (Figure 4a) [see also *Gerstoft et al.*, 2008], correlating well with ocean wave height [*Tolman*, 2005]. LPDF *P*-wave microseisms have a stronger coastal component (Figure 4b), generated along Pacific coastlines all year long. In summer, intense wave activity across the South Pacific dominates *P*-wave microseism generation in both bands. In winter, the North Atlantic is also a strong LPDF *P* source region. It is interesting that the Hawaiian Island chain seems to be a hotspot of coastal wave-wave interaction that generates LPDF *P*-wave microseisms in addition to surface waves [*Bromirski et al.*, 2005], as observed for each month in Figure 4b.

[15] For point sources at selected global locations (crosses in Figures 4c and 4d), we construct a synthetic beam neglecting amplitude differences, by modeling phase responses corresponding to the travel times at each station, i.e., $\sum_k \exp(i\omega \mathbf{t}_{lat[k],lon[k]})$, where $\mathbf{t}_{lat[k],lon[k]}$ describes the travel times from the k^{th} point source to each array stations. Excluding the Hawaiian Island chain, LPDF *P*-wave source areas are modeled for summer and winter months respectively (Figures 4c and 4d). The simulations do not show significant beamformer leakage near Hawaii, in contrast to the local maximum near Hawaii observed in the real data (Figure 4b). This indicates that the wave-wave interaction observed near Hawaii is not a processing artifact.

5. Conclusion

[16] Beamforming of land-based seismic array data shows clear evidence of deep-ocean origins of SPDF (0.16–0.35 Hz)

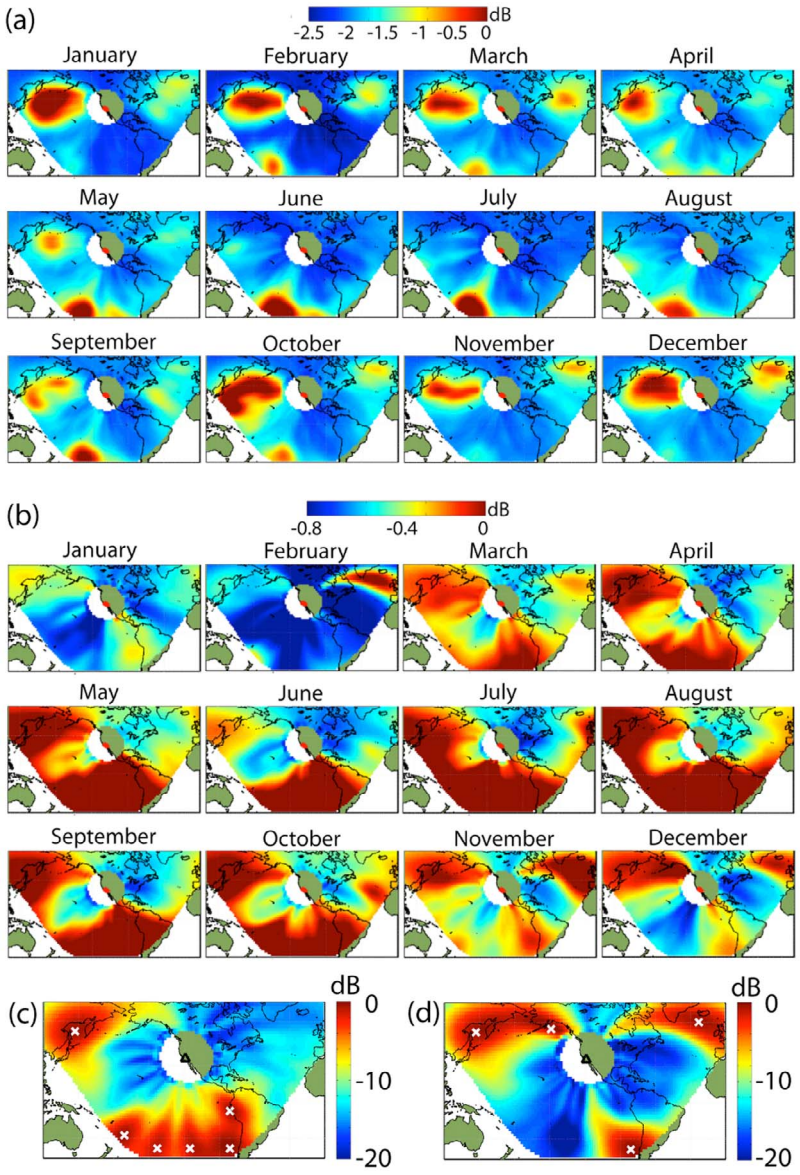

Figure 4. *P*-wave microseism source areas from monthly averaged beamformer outputs using the SCSN data in 2006. (a) SPDF (0.18–0.25 Hz) *P*-wave source areas. (b) LPDF (0.10–0.13 Hz) *P*-wave source areas. The dB scales are independent for SPDF and LPDF bands. (c) Synthetic LPDF *P*-wave beams for summer months, excited by spatially distributed point sources at selected locations (crosses). (d) Synthetics for winter months.

P-wave microseisms due to nonlinear wave-wave interactions of local wind seas near storms. Weaker *P*-wave microseisms are also observable in the LPDF (0.1–0.13 Hz) band, likely associated with swell interactions near the coastlines. These observations show that wave-wave interactions under tropical cyclones may be tracked using land-based seismic arrays.

[17] Surface waves generated under the storm were not observed. Further studies with higher density arrays are needed to conclusively determine if surface-wave DF microseisms generated in deep oceans are observed on land.

[18] **Acknowledgments.** This work was supported by U.S. Air Force Research Laboratory (FA8718-07-C-0005), Minerals Management Service via the Gulf of Mexico Hydrates Research Consortium, and California Department of Boating and Waterways (to PDB). Data were from Southern California Earthquake Data Center (http://www.data.scec.org/), and National Research Institute for Earth Science and Disaster Prevention (NIED) in Japan.

References

Bromirski, P. D. (2001), Vibrations from the "Perfect Storm," *Geochem. Geophys. Geosyst.*, *2*(7), 1030, doi:10.1029/2000GC000119.

Bromirski, P. D., and F. K. Duennebier (2002), The near-coastal microseism spectrum: Spatial and temporal wave climate relationships, *J. Geophys. Res.*, *107*(B8), 2166, doi:10.1029/2001JB000265.

Bromirski, P. D., F. K. Duennebier, and R. A. Stephen (2005), Mid-ocean microseisms, *Geochem. Geophys. Geosyst.*, *6*, Q04009, doi:10.1029/2004GC000768.

Burg, J. P., and G. C. Burrell (1967), Analysis of K-line wavenumber spectra from the TFO long noise sample, *Spec. Rep. AFTAC Proj. VT/4053*, Def. Tech. Inf. Cent., Fort Belvoir, Va.

Cessaro, R. (1994), Sources of primary and secondary microseisms, *Bull. Seismol. Soc. Am.*, *84*, 142–148.

Chevrot, S., M. Sylvander, S. Benahmed, C. Ponsolles, J. M. Lefevre, and D. Paradis (2007), Source locations of secondary microseisms in western Europe: Evidence for both coastal and pelagic sources, *J. Geophys. Res.*, *112*, B11301, doi:10.1029/2007JB005059.

Gerstoft, P., and T. Tanimoto (2007), A year of microseisms in southern California, *Geophys. Res. Lett.*, *34*, L20304, doi:10.1029/2007GL031091.

Gerstoft, P., M. C. Fehler, and K. G. Sabra (2006), When Katrina hit California, *Geophys. Res. Lett.*, *33*, L17308, doi:10.1029/2006GL027270.

Gerstoft, P., P. M. Shearer, N. Harmon, and J. Zhang (2008), Global *P*, *PP*, and *PKP* wave microseisms observed from distant storms, *Geophys. Res. Lett.*, *35*, L23306, doi:10.1029/2008GL036111.

Haubrich, R. A., and K. McCamy (1969), Microseisms: Coastal and pelagic sources, *Rev. Geophys.*, *7*, 539–571, doi:10.1029/RG007i003p00539.

Kedar, S., M. Longuet-Higgins, F. Webb, N. Graham, R. Clayton, and C. Jones (2008), The origin of deep ocean microseisms in the North Atlantic Ocean, *Proc. R. Soc. A.*, *464*, 777–793, doi:10.1098/rspa.2007.0277.

Kennett, B. L. N., E. R. Engdahl, and R. Buland (1995), Constraints on seismic velocities in the Earth from travel times, *Geophys. J. Int.*, *122*, 108–124, doi:10.1111/j.1365-246X.1995.tb03540.x.

Koper, K., and B. de Foy (2008), Seasonal anisotropy of short-period seismic noise recorded in South Asia, *Bull. Seismol. Soc. Am.*, *98*, 3033–3045, doi:10.1785/0120080082.

Koper, K. D., B. de Foy, and H. Benz (2009), Composition and variation of noise recorded at the Yellowknife Seismic Array, 1991–2007, *J. Geophys. Res.*, *114*, B10310, doi:10.1029/2009JB006307.

Landes, M., F. Hubans, N. M. Shapiro, A. Paul, and M. Campillo (2010), Origin of deep ocean microseisms by using teleseismic body waves, *J. Geophys. Res.*, *115*, B05302, doi:10.1029/2009JB006918.

Longuet-Higgins, M. S. (1950), A theory of origin of microseisms, *Philos. Trans. R. Soc. London, Ser. A*, *243*, 1–35, doi:10.1098/rsta.1950.0012.

Sabra, K. G., P. Gerstoft, P. Roux, W. A. Kuperman, and M. C. Fehler (2005), Surface wave tomography from microseisms in southern California, *Geophys. Res. Lett.*, *32*, L14311, doi:10.1029/2005GL023155.

Shapiro, N. M., M. Campillo, L. Stehly, and M. H. Ritzwoller (2005), High-resolution surface-wave tomography from ambient seismic noise, *Science*, *307*, 1615–1618, doi:10.1126/science.1108339.

Shearer, P. M. (2009), *Introduction to Seismology*, Cambridge Univ. Press, Cambridge, U. K.

Sutton, G. H., and N. Barstow (1990), Ocean-bottom ultralow-frequency (ULF) seismo-acoustic ambient noise: 0.002 to 0.4 Hz, *J. Acoust. Soc. Am.*, *87*, 2005–2012, doi:10.1121/1.399328.

Tanimoto, T. (2007), Excitation of microseisms, *Geophys. Res. Lett.*, *34*, L05308, doi:10.1029/2006GL029046.

Tanimoto, T., S. Ishimaru, and C. Alvizuri (2006), Seasonality in particle motion of microseisms, *Geophys. J. Int.*, *166*, 253–266, doi:10.1111/j.1365-246X.2006.02931.x.

Toksöz, N. M., and R. T. Lacoss (1968), Microseisms: Mode structure and sources, *Science*, *159*, 872–873, doi:10.1126/science.159.3817.872.

Tolman, H. L. (2005), Manual and wave user system documentation of WAVEWATCH-III, NOAA, Camp Springs, Md. (Available at http://polar.ncep.noaa.gov/)

Zhang, J., P. Gerstoft, and P. M. Shearer (2010), Resolving *P*-wave travel-time anomalies using seismic array observations of oceanic storms, *Earth Planet. Sci. Lett.*, *292*, 419–427, doi:10.1016/j.epsl.2010.02.014.

P. D. Bromirski, P. Gerstoft, and J. Zhang, Scripps Institution of Oceanography, University of California, San Diego, La Jolla, CA 92093-0238, USA. (jianz@ucsd.edu)